



CHORUS

This is the accepted manuscript made available via CHORUS. The article has been published as:

Surface-Emission Studies in a High-Field RF Gun based on Measurements of Field Emission and Schottky-Enabled Photoemission

H. Chen, Y. Du, W. Gai, A. Grudiev, J. Hua, W. Huang, J. G. Power, E. E. Wisniewski, W. Wuensch, C. Tang, L. Yan, and Y. You

Phys. Rev. Lett. **109**, 204802 — Published 14 November 2012

DOI: [10.1103/PhysRevLett.109.204802](https://doi.org/10.1103/PhysRevLett.109.204802)

Surface Emission Studies in a High Field RF Gun based on Measurements of Field Emission and Schottky Enabled Photoemission

H. Chen,¹ Y. Du,¹ W. Gai,² A. Grudiev,³ J. Hua,¹ W. Huang,¹ J. G. Power,²
E.E. Wisniewski,^{2,4,*} W. Wuensch,³ C. Tang,¹ L. Yan,¹ and Y. You¹

¹*Dept. of Eng. Phys., Tsinghua U., China*

²*ANL/HEP, Argonne, IL USA*

³*CERN, Geneva Switzerland*

⁴*IIT Chicago, IL USA*

(Dated: August 16, 2012)

We report on investigations into the fundamental surface emission parameters, the geometric field enhancement factor (β) and the work function (ϕ), by making both field emission and Schottky-enabled photoemission measurements. The measurements were performed on a copper surface in the Tsinghua University S-band RF gun in two separate experiments. Fitting our data to the models for each experiment indicate that the traditionally assumed high value of β ($\approx 50 - 500$) does not provide a plausible explanation of the data, but incorporating a low value of ϕ at some sites does. In addition, direct measurements of the surface conducted after the experiment show that β is on the order of a few, consistent with our understanding of the electron emission measurements. Thus we conclude that the dominant source of electron emission in high gradient RF cavities is due to low ϕ sites, as opposed to the conventionally assumed high β sites. The origin of low ϕ at these sites is unclear and should be the subject of further investigation.

RF breakdown in high-gradient accelerating structures is an important issue and is still poorly understood. Field emission (FE) is considered to be the major gradient limiting factor in RF cavities and a precursor to breakdown. FE is analyzed via Fowler-Nordheim (FN) theory using β and ϕ . Typically, ϕ is assumed constant and the onset of FE in RF cavities is attributed to small geometric surface imperfections such as peaks locally enhancing the applied electric field. Field enhancement is parametrized by a scaling factor β which is a measure of the microscopic surface roughness. The FN plot also allows the computation of the emitting area A_e . Given β and A_e , one could also calculate the work function.

In this letter we use two surface parameters, β and ϕ , to discuss and analyze FE and Schottky-enabled photoemission data from a RF photocathode gun. The traditional FN analysis of FE data in RF cavities holds constant the work function of the metal, ϕ . An alternative approach is to consider the local variation of ϕ across the surface along with β , an approach suggested by B.M. Cox [1] (see Fig. 1).

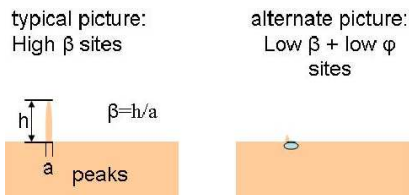


FIG. 1. The role of geometric perturbations (parametrized by β) vs. work function perturbations (parametrized by ϕ) and their relative weights should be considered in determining the onset of field emission.

Field emission and photoemission data was taken at

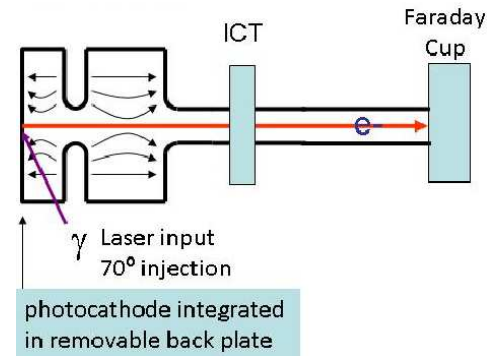


FIG. 2. Schematic of the experimental setup for FE and photoemission measurements at Tsinghua University.

the Tsinghua University S-band RF gun facility. The gun operates at 2856 MHz with a RF pulse length of 2 μ s. The laser has a fundamental wavelength of 800 nm and a 400 nm harmonic. Most RF photocathode guns have a removable photocathode plug in a central hole of the back wall. This setup results in dark current emitted from the edges in the gap between the photocathode and the wall which is hard to separate from the cathode emission. This dark current interferes with the electrons emitted from the surface that we are trying to measure. On the other hand, the Tsinghua RF gun by design is well-suited to surface emission current measurement (see schematic in Fig. 2). The back wall of the gun is a solid, de-mountable copper plate. The backplane of the gun, with a central diamond-polished area, serves as a photocathode. Observed electron emission comes only from the surface and not from edges around the cathode. The available RF field level is in the range 50-75 MV/m. For

a more detailed description of the gun, see [2], [3]. For the experiment, peak RF field was varied systematically from 57-73 MV/m. FE current was measured with a Faraday cup just outside the gun.

The FN equation predicts the FE current as a function of β and ϕ , $I_{FE}(\beta, \phi)$. The Schrodinger equation is solved for an E-field-modified surface potential at the surface of a metal[4],[5],[6]. Local field variations due to surface roughness are introduced via β such that $E_{local} = \beta E$ [7]. RF fields are introduced by substitution of $E = E \sin \theta$ (where θ =RF phase) and integrating over an RF period to derive the FN equation for RF fields [8]:

$$\bar{I} = \frac{5.7 \times 10^{-12} \times 10^{4.52\phi^{-0.5}} A_e (\beta E)^{2.5}}{\phi^{1.75}} \times e^{\left(\frac{-6.53 \times 10^9 \phi^{1.5}}{\beta E}\right)} \quad (1)$$

with I = the FE current in Amperes averaged over one RF period, ϕ =the work function (eV), E = peak surface electric field (V/m), A_e = emission area (m²), and β = the field enhancement factor.

The usual experimental approach is to take FE data using a Faraday cup or an Integrating Charge Transformer (ICT) (see Fig. 2), then plot current and RF field on a FN plot, which linearizes the exponential. After doing a linear fit, β is computed from the slope and the emitting area A_e from the intercept.

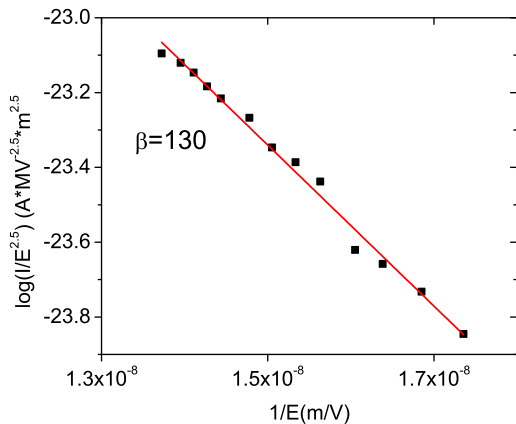


FIG. 3. Fowler-Nordheim plot of normalized FE data from the S-band RF gun. Applying traditional analysis, both the field enhancement factor $\beta=130$ and the emission area $A_e = 4 \text{ nm}^2$ were extracted from the slope of the plot using $\phi = 4.6 \text{ eV}$, bulk work function of copper.

The FE data is plotted and fitted in Fig. 3. Each point on the plot results from the average of 6-10 measurements with $\bar{\sigma} \approx 3\%$. The adjusted R-squared for the linear fit was 0.99. β was extracted using the typical FN approach assuming the bulk work function of copper, $\phi = 4.6 \text{ eV}$, and yielding $\beta = 130$, consistent with typical RF cavity FE data [9],[10],[8]. The emission area $A_e \approx 4 \text{ nm}^2$ was also extracted from the fit.

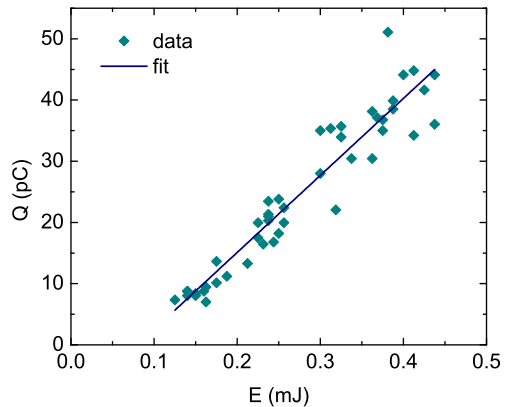


FIG. 4. Schottky-enabled photoemission data from the S-band RF gun. Long pulse (3 ps). $h\nu = 3.1 \text{ eV}$, $E_{peak} = 55 \text{ MV/m}$, injection phase = 80° , $E_{accel} = 54 \text{ MV/m}$. Data with linear fit.

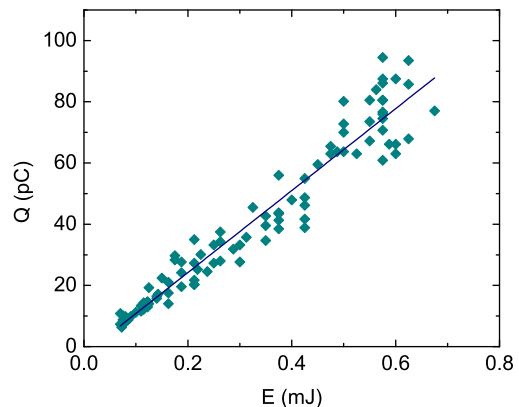


FIG. 5. Schottky-enabled photoemission data from the RF gun. Short pulse (0.1 ps). $h\nu = 3.1 \text{ eV}$, $E_{peak} = 55 \text{ MV/m}$, injection phase = 80° , $E_{accel} = 54 \text{ MV/m}$. Data with linear fit.

The threshold for photoemission current in RF guns, similar to FE current, is also a function of the surface parameters ϕ and β . This threshold is probed with Schottky-enabled photoemission which involves using a photon energy ($h\nu$) below the photoemission threshold and raising the Electric field to probe the threshold. A detailed discussion of the method is available here[12]. Photocathode RF guns normally operate with $h\nu \gg \phi$ of the cathode. For the Schottky-enabled photoemission experiment, the parameters used were: bulk work function of Cu = $\phi = 4.6 \text{ eV}$, $h\nu = 3.1 \text{ eV}$. The difference between the photon energy and ϕ is 1.5 eV. The threshold condition for Schottky-enabled photoemission is this: the absolute difference between ϕ and $h\nu$ is equal to the Schottky potential. The expression for Schottky-

enabled photoemission at the photoemission threshold can be written[12]:

$$h\nu \approx \phi - \sqrt{e^3\beta E 4\pi\epsilon_0} \quad (2)$$

where β = the field enhancement factor, $h\nu$ =the photon energy in eV, ϕ =the bulk work function, E = peak surface electric field and ϵ_0 is the vacuum permittivity. The radical expression is the E-field induced work function reduction due to the Schottky effect. To meet the threshold condition requires high E-field, high β or low ϕ (or combination).

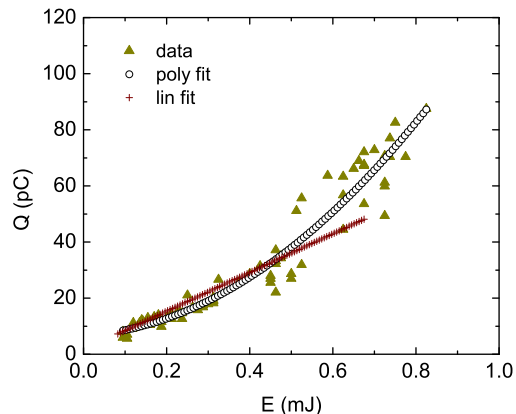


FIG. 6. $E_{peak} = 50$ MV/m, injection phase = 30° , $E_{accel} = 25$ MV/m. Schottky-enabled photoemission, near threshold. The plot becomes non-linear at laser energy above 0.4mJ, indicative of the multi-photon emission regime. Data with laser energy < 0.4 mJ with linear fit, data with laser energy > 0.4 mJ, quadratic fit.

In case 1, the peak accelerating E-field was high (54 MV/m) and only single photon emission was observed; see Figs. 4 and 5. Two laser pulse lengths, long (3 ps) and short (0.1 ps), were used to determine if multi-photon emission, which could obscure the single photon emission signal, was occurring during the measurement. The expectation is that while operating within the single-photon emission regime, both pulse lengths will yield the same charge at a given laser energy and remain linear. The results in Fig. 4 and 5 appear linear and have a similar Quantum Efficiency (QE), indicating single-photon emission. The QE extracted from the fits for the plots appears low as emission does not occur equally at all points in the laser spot. Rather, we believe most of the emission is coming from some small, high QE sites within the laser spot. In addition, since the laser energy is measured with a photodiode outside the vacuum window, there are losses due to attenuation and reflection losses at the window and the laser mirror inside the vacuum chamber. These losses are the reason that the y-intercept is offset from the origin. The QE from Fig. 4

was about $3.90 \pm 0.18 \times 10^{-7}$. The QE from Fig. 5 was $4.15 \pm 0.11 \times 10^{-7}$, about the same.

In case 2, the peak accelerating E-field was low (25 MV/m) and approaching the threshold for Schottky-enabled photoemission, but also approaching the instrumentation limits. Fig. 6 shows an initial linear trend which becomes quadratic as the laser energy increases above 0.4 mJ. This is indicative of the onset of two-photon emission at high laser intensity. The QE calculated from the slope of the linear region was $3.11 \pm 0.11 \times 10^{-7}$. The adjusted R-squared for the linear fits were as follows: Fig. 4, 0.905; Fig. 5, 0.94; and 6, 0.904. The standard error was $\leq 5\%$.

Schottky-enabled photoemission was observed at all measured field levels. Using equation 2, with a field level of 54 MV/m together with the bulk ϕ of Cu = 4.6 eV, a lower limit on $\beta \approx 30$ was obtained from the data in Fig. 4 and 5. Taking the lowest field level at which emission was measured ($E=25$ MV/m), together with the bulk work function of Cu, an approximate upper limit on $\beta \approx 60$ may be obtained. However, the signal in the low-field case was weak and noisy so the actual threshold could be higher or lower, and therefore so could β .

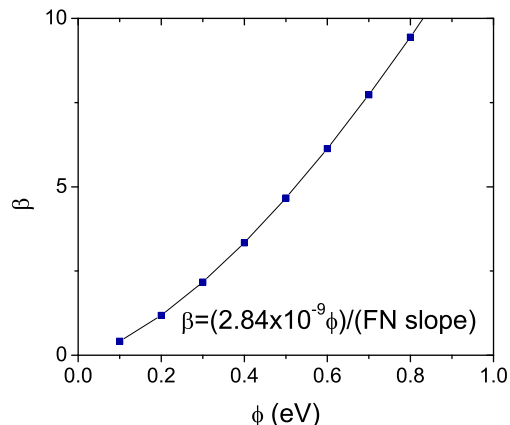


FIG. 7. β vs ϕ plotted using the slope of the FN plot for the Tsinghua data (Fig. 3). Each point on the plot represents a possible combination of field enhancement factor and local work function which match the data.

The high β values we computed using both the FN approach and the Schottky-enabled photoemission measurements are unphysical, as we now explain. For a surface machined to ≈ 10 nm roughness, typical in a RF cavity, this implies emission from tall, thin features resembling 10 nm stacks of atoms. Such a tower of atoms would have an aspect ratio of 100:1. Surface analysis has shown these type of features simply are not there. There are many reports of other researchers who have had difficulty finding evidence of high β geometric features [13],[9],[14]. In an effort to explain this, some have postulated other mechanisms, for example, [15]. Results

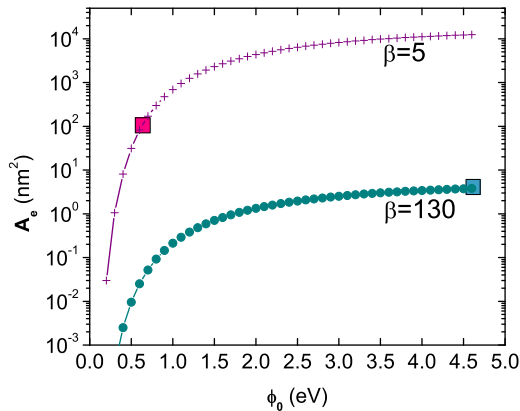


FIG. 8. Emitting area A_e computed from the intercept of the FN plot (Fig. 3) using two different values of β . The squares indicate the two points we chose for the purpose of comparison.

of extensive studies of FE in Niobium cavities at Cornell, Saclay and Orsay published in the early 1990s reported contaminants, rather than surface projections, as a primary source of FE current[16],[10],[17].

If one assumes a perfect metal surface, then in order for field emission to occur, the local field has to be very high, $E=O(\text{GV}/\text{m})$, requiring a large value of β . However, surface analysis of the cathode using white-light interferometry to determine surface roughness did not discover features that could account for such a high β . In fact, the maximum value of β reported by Qian et al was only about 1.2 [11], more than two orders of magnitude smaller than the field enhancement from FN analysis. In addition, we also have the data from Schottky-enabled photoemission which indicates $\beta \gg 30$. The difference between the two could be due to the fact that the laser samples only a small part of the cathode surface while FE is from the entire surface. Since both results are inconsistent with the surface analysis, we think a more plausible view is that emission is from a few small locally low ϕ sites.

An alternative way to fit the data is to use a lower value of β (≈ 5), and assume that some unknown defect or mechanism lowers the work function at each point of emission. In other words, a distribution which includes a few sites of low ϕ exists on the surface. In our view, it is these low work function sites which set the threshold level for field emission and Schottky-enabled photoemission.

To explore the idea that the work function may vary considerably at small areas across the surface, we looked at the effect of different combinations of local ϕ and β . We found it possible to fit the same data with a Fowler Nordheim plot in many ways (Fig. 7). Each point on the plot represents a (ϕ, β) pair based on the data and satisfying the FN theory. However, only low β sites satisfy

the surface analysis results reported in Ref. [11].

In addition to the field enhancement factor, another quantity which may be extracted from a FN plot is the total area of emission, A_e . The area calculated in this way is typically so small that observation is problematic and the resulting current density unphysically high. From Fig.8, choosing the point on the curve which represents the typical FN approach applied to the data, $(\phi, \beta) = (4.6, 130)$, it can be seen that the total emission area is extremely small, $A_e \approx 4 \text{ nm}^2$. Based on the data, an area of this size would have a current density of about $4 \times 10^9 \text{ A}/\text{cm}^2$.

Because the calculated current density is in the resistive heating regime, we did a simple-minded calculation of the expected temperature rise due to Joule heating of the emission site, neglecting heat conduction away from the site. Using the RMS current, the emission area and material constants, Joule heating calculation yields a temperature rise of $500,000^\circ\text{C}$, per 100 ns of RF, far beyond the melting point of copper. Using our alternate approach, we choose the point on the upper curve $(\phi, \beta) = (0.5, 5)$ which gives a much more reasonable $A_e \approx 100 \text{ nm}^2$. Doing the same calculation with this area results in a more moderate temperature increase of 800°C . Choosing another point on the curve, $(\phi, \beta) = (2.5, 5)$ yields $A_e \approx 5000 \text{ nm}^2$, which would result in a negligible temperature increase. This type of calculation, while very qualitative, does suggest that the usual analysis does not work.

It is also observed that melting of emitters during RF processing often results in increased surface roughness. This should mean higher β and higher FE but the reality is that after RF processing, FE declines[14]. This contradiction can be explained by initially low work function emitter sites which are melted, transforming them into high work function sites with increased β , but the net effect is decreased FE.

In conclusion, we have characterized ϕ and β using field emission and photoemission from an S-band RF photocathode gun. We believe that a cross-check of the data indicates that using a low ϕ and reasonable $\beta \approx 5$ explains the data better than the usual approach assuming constant material work function with a very high β . In this view, low ϕ sites are responsible for field emission and are potential RF breakdown sites. While low ϕ sites have not been directly identified, the existence of high β sites has been ruled out by surface analysis. In the future, systematic surface studies at the nanometer scale are required in order to give a definitive explanation.

This work was funded by the U.S. Dept of Energy Office of Science under contract number DE-AC02-06CH11357.

* ewisniew@hawk.iit.edu

- [1] B. M. Cox, *Journal of Physics D: Applied Physics* **8**, 2065 (1975).
- [2] Y.-C. Du, L.-X. Yan, Q. Du, X.-Z. He, D. Xiang, C.-X. Tang, W.-H. Huang, and Y.-Z. Lin, *Chinese Physics Letters* **24**, 1876 (2007).
- [3] Y. Du, L. Yan, D. Xiang, W. Huang, C. Tang, and Y. Lin, in *Particle Accelerator Conference, 2007. PAC. IEEE* (2007) pp. 1043–1045.
- [4] R. H. Fowler and L. Nordheim, *Proceedings of the Royal Society of London. Series A* **119**, 173 (1928).
- [5] E. L. Murphy and R. H. Good, *Phys. Rev.* **102**, 1464 (1956).
- [6] Richard G. Forbes and Jonathan H.B Deane, *Proceedings of the Royal Society A: Mathematical, Physical and Engineering Science* **463**, 2907 (2007).
- [7] D. Alpert, D. A. Lee, E. M. Lyman, and H. E. Tomaschke, *Journal of Vacuum Science and Technology* **1**, 35 (1964).
- [8] J. Wang and G. Loew, *Field emission and RF breakdown in high-gradient room-temperature linac structures*, Tech. Rep. SLAC-PUB-7684 (SLAC, 1997).
- [9] U. Klein and J. Turneaure, *IEEE Transactions on Magnetics* **19**, 1330 (1983).
- [10] J. Tan, H. Safa, B. Bonin, and M. Jimenez, *Journal of Physics D: Applied Physics* **27**, 2654 (1994).
- [11] H. J. Qian, C. Li, Y. C. Du, L. X. Yan, J. F. Hua, W. H. Huang, and C. X. Tang, *Phys. Rev. ST Accel. Beams* **15**, 040102 (2012).
- [12] Z. M. Yusof, M. E. Conde, and W. Gai, *Phys. Rev. Lett.* **93**, 114801 (2004).
- [13] R. J. Noer, *Applied Physics A: Materials Science & Processing* **28**, 1 (1982), 10.1007/BF00617778.
- [14] S. Kobayashi, Y. Saito, T. Mizusawa, K. Shirai, R. Latham, K. Tajiri, and Y. Yamanaka, *Applied Surface Science* **144 - 145**, 118 (1999).
- [15] H. A. Schwettman, J. P. Turneaure, and R. F. Waites, *Journal of Applied Physics* **45**, 914 (1974).
- [16] D. Moffat, P. Barnes, t. Flynn, J. Graber, L. Hand, W. Hartung, T. Hays, J. Kirchgessner, j. Knobloch, R. Noer, H. Padamsee, D. Rubin, and J. Sears, in *Particle Accelerators*, Vol. 40 (Gordon and Breach, 1992) pp. 85–126.
- [17] J. Tan, in *Particle Accelerators*, Vol. 53 (Gordon and Breach, 1996) pp. 1–34.